AIP Advances

Ternary VS_2/ZnS/CdS hybrids as efficient electrocatalyst for hydrogen evolution reaction: Experimental and theoretical insights

Cite as: AIP Advances **11**, 105010 (2021); https://doi.org/10.1063/5.0068407
Submitted: 25 August 2021 . Accepted: 26 September 2021 . Published Online: 08 October 2021

Pratik V. Shinde, Deepak S. Gavali, Ranjit Thapa, et al.

Ternary VS_2/ZnS/CdS hybrids as efficient electrocatalyst for hydrogen evolution reaction: Experimental and theoretical insights

Cite as: AIP Advances 11, 105010 (2021); doi: 10.1063/5.0068407
Submitted: 25 August 2021 • Accepted: 26 September 2021 •
Published Online: 8 October 2021

Pratik V. Shinde,[1] Deepak S. Gavali,[2] Ranjit Thapa,[2] Manoj Kumar Singh,[3,a)] and Chandra Sekhar Rout[1,a)]

AFFILIATIONS

[1] Center for Nano and Material Sciences, Jain University, Jain Global Campus, Jakkasandra, Ramanagaram, Bangalore 562112, Karnataka, India
[2] Department of Physics, SRM University-AP, Amaravati 522240, Andhra Pradesh, India
[3] Department of Physics Under School of Engineering and Technology (SOET), Central University of Haryana (CUH), Mahendergarh 123031, Haryana, India

Note: This paper is part of the AIP Advances Special Collection on Advances in Low Dimensional and 2D Materials.
[a)]**Authors to whom correspondence should be addressed:** manojksingh@cuh.ac.in and r.chandrasekhar@jainuniversity.ac.in

ABSTRACT

Widely used precious metal (i.e., Pt, or Pd) electrocatalysts need to be replaced with other cost-effective and earth-abundant materials for economical water splitting applications. Recently, two-dimensional (2D) transition metal dichalcogenides (MoS_2, VS_2, WS_2, etc.) have emerged as ideal electrocatalysts for the hydrogen evolution reaction (HER) due to their tunable physicochemical properties and rich catalytic active sites. In this regard, we propose a strategy to achieve improved HER performance of VS_2 by fabricating a hybrid material with transition metal (Zn and Cd)-based sulfides. A facile hydrothermal approach is employed to prepare a VS_2/ZnS/CdS hybrid catalyst that exhibits remarkable electrocatalytic performance for the HER in acidic media with a small overpotential of 86 mV at 10 mA/cm^2 and a Tafel slope of 74.4 mV/dec. This inferred the Volmer–Heyrovsky mechanism with electrochemical desorption of hydrogen as the rate-limiting step. High performance is attributed to the abundance of catalytically active sites and the synergistic interactions between the materials. Theoretical calculations reveal that the VS_2/ZnS/CdS hybrid shows favorable HER activity owing to its low hydrogen adsorption free energy of about 0.35 eV. We believe that this work on designing 2D VS_2/ZnS/CdS will offer a new pathway to discover an efficient H_2 generation electrocatalyst.

I. INTRODUCTION

Persistently increasing global energy demands and simultaneous shrinkage of conventional fuel sources stimulated enormous research focus on the development of technologies for sustainable energy conversion and storage. Water splitting is one of the promising approaches to decode this energy glitch than other existing ones.[1] Hydrogen (H_2) is considered as green, recyclable energy and reflecting all norms for an alternative energy source.[2] Despite that, the efficient use of this eco-friendly technology needs to be enhanced by resolving the enigmas associated with it. The electrochemical splitting of water molecules transpired to the oxygen evolution reaction (OER) at the anode and the hydrogen evolution reaction (HER) at the cathode. Water splitting in acidic media has been recognized as the primary method of H_2 generation.[3] In the acidic electrolyte, the key steps are illustrated as a hydronium cation (H_3O^+) absorbed on a catalytic active site and coupled with an electron to form a hydrogen atom.[4] These processes required an efficient electrocatalyst to promote sluggish kinetics. Thus, for large-scale commercialization of H_2 production, more enhancement is needed in the extent of electrocatalyst due to its direct affection on the overall performance of water splitting.

Due to the suitable hydrogen adsorption (H_{ads}) energy on the catalytic active sites of platinum (Pt)-based materials, Pt has been used as the expediting electrocatalyst for the HER.[5] However, the use of this precious metal for HER application is hindered because of its high cost and scarcity on the earth's surface. Therefore, to make HER more productive, the discovery of alternative efficient material with high catalytic activity, cost-effective, and durable electrocatalyst is highly crucial.[6] Among the various non-precious metal-based electrocatalysts, transition metal sulfides have emerged as the superior HER electrocatalysts in recent years.[7] The advantageous properties, such as good conductivity, low cost, less environmental impact, and considerable catalytic activity toward the electrochemical HER, make them promising candidates. One of the classes of 2D materials, transition metal dichalcogenides (TMDCs), constitute by sandwiching transition metals (M–Mo, V, W, Re, etc.) in two chalcogen atoms (X–S, Se, or Te) with covalent bonding. The layers are connected with each other by weak van der Waals forces. Such a layered structure leads to strong anisotropy in its electrical, optical, chemical, and thermal properties. Depending on their variety of shapes, sizes, crystalline forms, chemical compositions, and structural configurations, they exhibit diverse properties ranging from insulators (e.g., HfS_2), semiconductors (e.g., MoS_2 and VS_2), semimetals (e.g., WTe_2 and $TiSe_2$), true metals (e.g., NbS_2 and VSe_2), and superconductors (e.g., $NbSe_2$ and TaS_2).[8] As a representative candidate of the TMDC family, the structure of vanadium disulfide (VS_2) is shaped by sandwiching a metal V-layer between two S-layers with an interlayer spacing of 5.76 Å.[9] VS_2 exhibits a small bandgap partly filled at the Fermi level, attractive metallic behavior with high electrical conductivity, high specific surface area, and unique mechanical properties.[10] Due to these several fascinating properties, VS_2 has become a superior candidate for facilitating various electrochemical applications, including supercapacitors, batteries, and electrocatalytic water splitting.[11–13] Significant effort has been devoted toward manufacturing, designing, and developing VS_2-based HER electrocatalysts. On the other hand, metal monosulfides (e.g., CdS, ZnS, NiS, and SnS) have attracted attention as a new class of electrode materials for electrochemical applications.[14,15] Cadmium sulfide (CdS) and zinc sulfide (ZnS) possess good electrical conductivity, low toxicity, natural abundance, low cost, and environmental stability. Both CdS and ZnS are semiconductors with a bandgap of 2.4 and 3.5–3.8 eV, respectively.[16,17] Such beneficial properties of both materials prompted researchers to exploit their potential in energy devices.

Design and fabrication of new hybrid nanostructures with strategic architectures are highly desirable due to the synergetic effect arising from the cooperation between two or multiple components that could lead to enhanced electrochemical properties.[18] Recently, hybrids or heterostructures engineered with transition metal sulfides have shown significant improvement in electrochemical performance from their single-component counterparts.[19,20] Herein, VS_2/ZnS/CdS hybrids were synthesized by a simple hydrothermal method. Impressively, the VS_2/ZnS/CdS hybrid exhibited outstanding electrocatalytic HER activity with a small overpotential of 86 mV at a current density of 10 mA/cm^2 and a Tafel slope of 74.4 mV/dec. The enhanced HER performance is attributed to the synergistic effect of VS_2 nanosheets and ZnS/CdS structures, which greatly promoted interfacial electronic and chemical interactions. Moreover, theoretical calculations reveal that the VS_2/ZnS/CdS hybrid structure is favorable in HER activity due to its low hydrogen adsorption free energy, which is about 0.35 eV. These fruitful outcomes evidence that the fabrication of optimized hybrid nanostructures is a promising strategy to enhance the catalytic performance of VS_2 material. Thus, these precious metal-free and highly active catalysts for the HER enable prospective opportunities for 2D materials in industrial applications.

II. EXPERIMENTAL SECTION

A. Chemicals

All the chemicals used in the study were of analytical grade and used without any further purification. The initial precursors such as NH_4VO_3, $Zn(NO_3)_2{\cdot}6H_2O$, $Cd(NO_3)_2{\cdot}4H_2O$, CH_4N_2S, ammonia, and H_2SO_4 were purchased from Sd-fine chemicals, India. C_2H_5NS was purchased from Sisco research laboratories (SRL), India. 20% Pt/C, Nafion, and isopropanol were purchased from Sigma-Aldrich. The deionized water (DI) was used to prepare the experimental solution and analyte solution.

B. Synthesis of ZnS/CdS structures

Typically, $Zn(NO_3)_2{\cdot}6H_2O$ (0.297 g) and $Cd(NO_3)_2{\cdot}4H_2O$ (0.236 g) were dissolved in DI water (35 ml) under vigorous stirring to form a homogeneous solution. Subsequently, CH_4N_2S (0.380 g) was added to the solution and stirred for another one hour. Then, the prepared solution was transferred into a 50 ml Teflon-lined stainless-steel autoclave and maintained at 180 °C for 24 h. After the reaction system cools down to room temperature, the precipitate was collected, washed with water and absolute ethanol several times to remove any possible impurities, and dried at 60 °C for 12 h under vacuum. Pristine ZnS and CdS materials were also obtained under the same procedure using their respective precursors.

C. Synthesis of VS_2/ZnS/CdS hybrid structures

NH_4VO_3 (0.696 g) was added to a 25 ml mixed solution of DI water and ammonia mixture. The solution was stirred for 15 min followed by adding 2.4 g C_2H_5NS and the mixture was stirred for 30 min. In another beaker, the as-prepared ZnS/CdS material was added into 15 ml of DI solution (1.0 mg/ml) and vigorously stirred for 30 min followed by ultrasonication. Then, the prepared solution was added to the above solution and further stirred for 30 min. The prepared homogeneous mixture was transferred into a 50 ml Teflon-lined stainless-steel autoclave to react at 180 °C for 24 h. After cooling down to ambient temperature, the product was centrifuged with DI water and ethanol. The VS_2/ZnS/CdS hybrid was eventually gathered after being dried at 60 °C at 6 h in a vacuum drying oven. For comparison purposes, pristine VS_2 was also synthesized by the same procedure.

D. Characterization

Fourier transform infrared (FTIR) spectra were acquired on a Perkin Elmer spectrophotometer to find the information about the functional groups present in the prepared materials. XRD was carried out by a Rigaku Ultima IV x-ray diffractometer having Ni-filter for Cu K_α radiation (wavelength, λ = 0.1541 nm) to understand the phase formation and crystallinity of the synthesized materials.

To study the phase constitution, x-ray photoelectron spectroscopy (XPS) measurements were performed using VG Microtech, England (Multi Lab, ESCA-3000, sr. no. 8546/1) with Al K_α as the x-ray source. Field-emission scanning electron microscopic (FESEM, JEOL JSM-7100F, JEOL Ltd., Singapore) and transmission electron microscopic [TEM, TALOS F200S G2 (200 kV, FEG CMOS camera 4 × 4 k^2)] measurements were employed to characterize the morphologies of the obtained samples. Selected area electron diffraction (SAED) patterns were collected on the same TEM instrument. The energy dispersive spectrometer (EDS) is also equipped with the same FESEM instrument and used for the elemental analysis of the material. The specific surface area and pore size distribution were measured by the multipoint Brunauer–Emmett–Teller (BET) and the Barrett–Joyner–Halenda (BJH) methods using Belsorp max, Japan.

E. Computational study details

We have performed the first-principles calculation based on density functional theory (DFT) implemented in the Vienna *ab initio* simulation package (VASP).[21] For all the calculations, we have used a projector augmented wave (PAW) scheme to project the potential of atoms, and the exchange–correlation energy was introduced by Perdew, Burke, and Ernzerhof (PBE).[22] For all the calculations, we have the kinetic energy cutoff of 450 eV and all the structure well optimization up to total energy and force conversion lower than 10^{-5} eV per atom and 0.001 eV/Å, respectively. To avoid the interaction of repeated images in the z-axis, we have used 20 Å of vacuum along the z-axis. The Brillion zone is defined by Monkhorst and Pack scheme 5 × 5 × 1 k-mesh in reciprocal space. To defined van der Waal's interaction, we have used Grimme's DFT-D2 method.[23]

F. Electrochemical measurements

All of the electrochemical measurements were performed in a three-electrode system on the CorrTest (CS350) Electrochemical Workstation, China. The Ag/AgCl electrode was used as the reference electrode, platinum was used as the counter electrode, and a glass carbon electrode (GCE, 3 mm in diameter) decorated with the catalysts was used as the working electrode. Typically, 2 mg of catalyst and 10 μl of Nafion solution were dispersed in 200 μl isopropanol solution by sonicating for 60 min to form a homogeneous ink. Then, 5 μl of the ink was pipetted onto a GCE. All HER tests were conducted in 0.5M H_2SO_4 electrolyte.

Linear sweep voltammetry (LSV) was conducted with a scan rate of 5 mV/S. All results were calibrated with respect to the reversible hydrogen electrode (RHE) according to the following equation:[24]

$$E_{(vs.\ RHE)} = E_{(vs.Ag/AgCl)} + 0.197 + 0.059\ pH. \quad (1)$$

Tafel plots of various samples were investigated using the following equation:[25]

$$\eta = b \log j + a, \quad (2)$$

where η is the overpotential, j is the current density, and b is the Tafel slope.

The electrochemical impedance spectroscopy (EIS) measurements were carried out in the frequency range of 0.01 Hz–100 kHz with an AC voltage of 5 mV. Cyclic voltammograms (CV) of the as-prepared samples were recorded in a non-Faradaic region at various scan rates used to measure the electrochemical double-layer capacitance (C_{dl}). Stability tests were performed using a chronoamperometry technique (at a current density of 10 mA/cm^2).

III. RESULTS AND DISCUSSION

We have developed a simple and effective strategy to fabricate the VS_2/ZnS/CdS hybrid structures with excellent electrocatalytic HER properties. The synthesis process of VS_2/ZnS/CdS hybrid structures is schematically illustrated in Fig. 1. Initially, structural and morphological analyses of synthesized materials were carried out by using various characterization techniques.

The FTIR analysis was carried out to analyze the composition and quality in the range of 4000–500 cm^{-1}, shown in Fig. 2(a). The dips observed around 600 cm^{-1} are due to the characteristic metal–sulfide (M–S) vibration. Additional peaks that appeared at 3400 cm^{-1} are attributed to the stretching vibration of the hydroxyl group (O–H). In order to determine the phase and purity of the synthesized materials, XRD analyses have been performed to understand structural information [Fig. 2(b)]. The XRD pattern of pristine CdS exhibits several characteristic peaks corresponding to the (100), (002), (101), (102), (110), etc., planes of hexagonal CdS (JCPDS card No. 65-3414). The peaks of cubic ZnS (JCPDS card No. 05-0566) match the crystal faces (111), (200), (220), (311), and (331). The XRD spectrum of ZnS/CdS clearly presented the planes of both ZnS and CdS material. Pure VS_2 is assigned to a hexagonal phase of VS_2 (JCPDS card No. 89-1640) and assigned to the crystal faces (001),

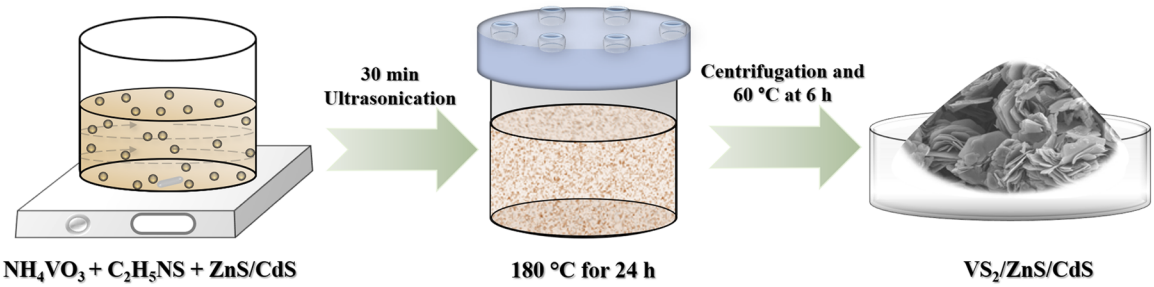

FIG. 1. Schematic illustration of the synthesis process of VS_2/ZnS/CdS hybrid.

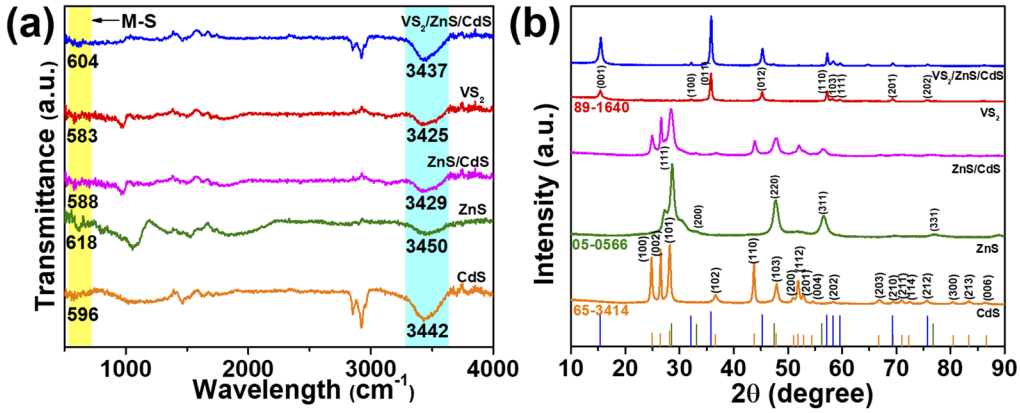

FIG. 2. (a) FTIR and (b) XRD patterns of synthesized materials.

(100), (011), (012), (110), (103), (111), (201), and (202). In the XRD pattern of the VS_2/ZnS/CdS hybrid, no intense peaks for the ZnS and CdS are observed, which is presumably due to the low content of the ZnS/CdS. For all the materials, no extra peaks are observed other than JCPDS files, representing that the as-synthesized samples are highly pure. EDS is a well-known method for identifying the relative elemental composition of a material. Figures S1a–S1f show the typical EDS mapping image of a VS_2/ZnS/CdS hybrid, which confirms the presence of V, Zn, Cd, and S elements in the sample. The chemical states of V, Zn, Cd, and S in the as-prepared VS_2/ZnS/CdS hybrid structure were investigated by the XPS. Figure S2 confirms the element of VS_2/ZnS/CdS hybrid with the peaks of V, Zn, Cd, and S elements. Figure 3(a) shows the V 2p core-level spectrum in which doublet peaks at the higher binding energy of 524.5 and 517.6 eV are

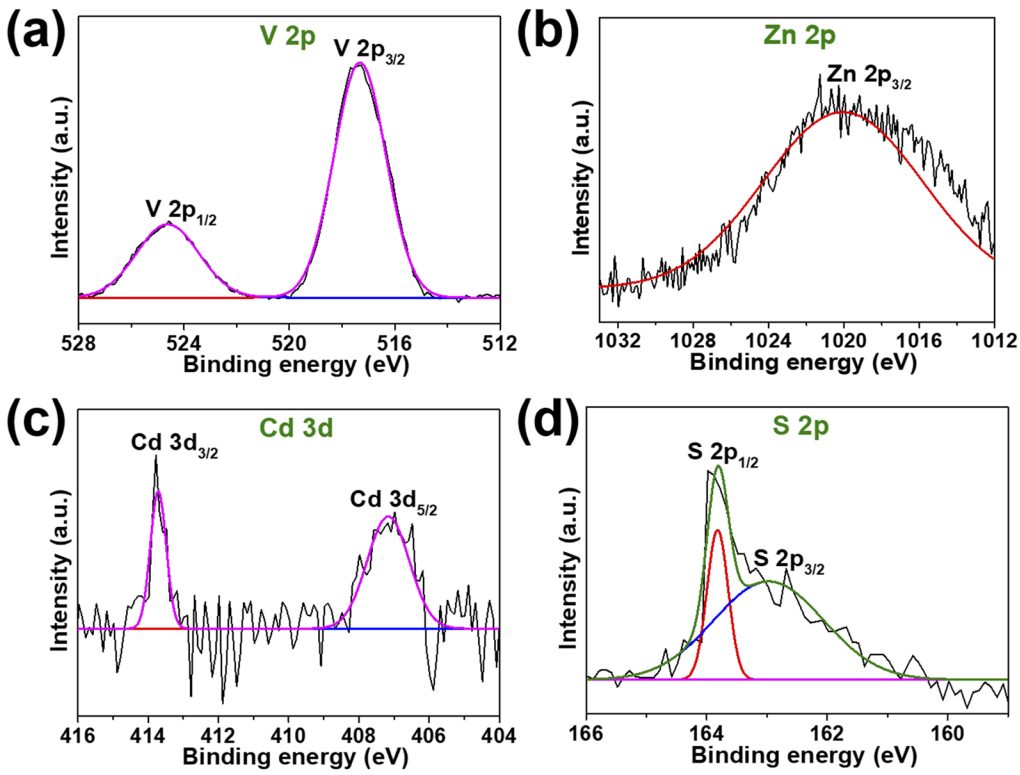

FIG. 3. High-magnification XPS spectra of VS_2/ZnS/CdS: (a) V 2p, (b) Zn 2p, (c) Cd 3d, and (d) S 2p.

attributed to V $2p_{1/2}$ and V $2p_{3/2}$, corresponding to the V^{4+} chemical state.[26] In Fig. 3(b), the high-resolution XPS spectra of Zn 2p, the peak at 1020.25 eV assigned to Zn $2p_{3/2}$, indicated the oxidation state of +2 for Zn.[27,28] The two peaks of Cd ($3d_{3/2}$ and $3d_{5/2}$) are located at 413.7 and 407.1 eV, respectively, which indicated the existence of Cd^{2+} [Fig. 3(c)].[29,30] From the high-resolution S 2p XPS spectrum in Fig. 3(d), the peak at 163.8 eV is ascribed to S $2p_{1/2}$, while the peak at 162.6 eV could be assigned to S $2p_{3/2}$.[31] These observations confirm the successful synthesis of the VS_2/ZnS/CdS hybrid material.

The morphology of the VS_2/ZnS/CdS hybrid is confirmed by SEM and TEM, as shown in Fig. 4. It can be seen from Figs. 4(a) and 4(b) that the morphology of CdS is flower-like structure, while ZnS has a spherical structure. The ZnS/CdS hybrid exhibits both the flower and spherical structures [Fig. 4(c)]. Figures 4(d) and 4(e) show low- and high-magnification FESEM images of vertically aligned VS_2 nanosheets. Figure 4(f) shows the FESEM images of the VS_2/ZnS/CdS hybrid, which represent the fragmented sheets dominated by the morphology of VS_2, due to the presence of a lower concentration of ZnS and CdS. TEM and HRTEM images of the VS_2/ZnS/CdS hybrid are shown in Figs. 4(g) and 4(h). The clear lattice fringes with interplanar spacings of 0.19, 0.34, and 0.31 nm correspond to (012), (002), and (111) planes of VS_2, CdS, and ZnS, respectively. The SAED pattern [Fig. 4(i)] clearly defines the semi-crystalline nature of the synthesized VS_2/ZnS/CdS hybrid and analyzes planes indexed as (102), (111), and (110), which correspond to CdS, ZnS, and VS_2. The surface area of the VS_2/ZnS/CdS hybrid structure is further investigated by combined nitrogen adsorption/desorption isotherms. Figure S3 shows a specific area of 4.3 m^2/g of VS_2/ZnS/CdS hybrid determined by the BET method, while pristine VS_2 shows 8.4 m^2/g and ZnS/CdS shows 6.5 m^2/g. The pore-size distribution curves are analyzed through the BJH method (Fig. S3). The corresponding pore volume of VS_2, ZnS/CdS, VS_2/ZnS/CdS hybrid is 0.017, 0.020, and 0.012 cm^3/g, respectively. All the above characterizations confirm the successful synthesis of the VS_2/ZnS/CdS hybrid.

The catalytic performance of the synthesized catalyst is measured by a three-electrode system in a 0.5M H_2SO_4 aqueous solution. Figure 5(a) shows the polarization curves of the as-prepared samples, CdS, ZnS, ZnS/CdS, VS_2/ZnS/CdS, and reference commercial

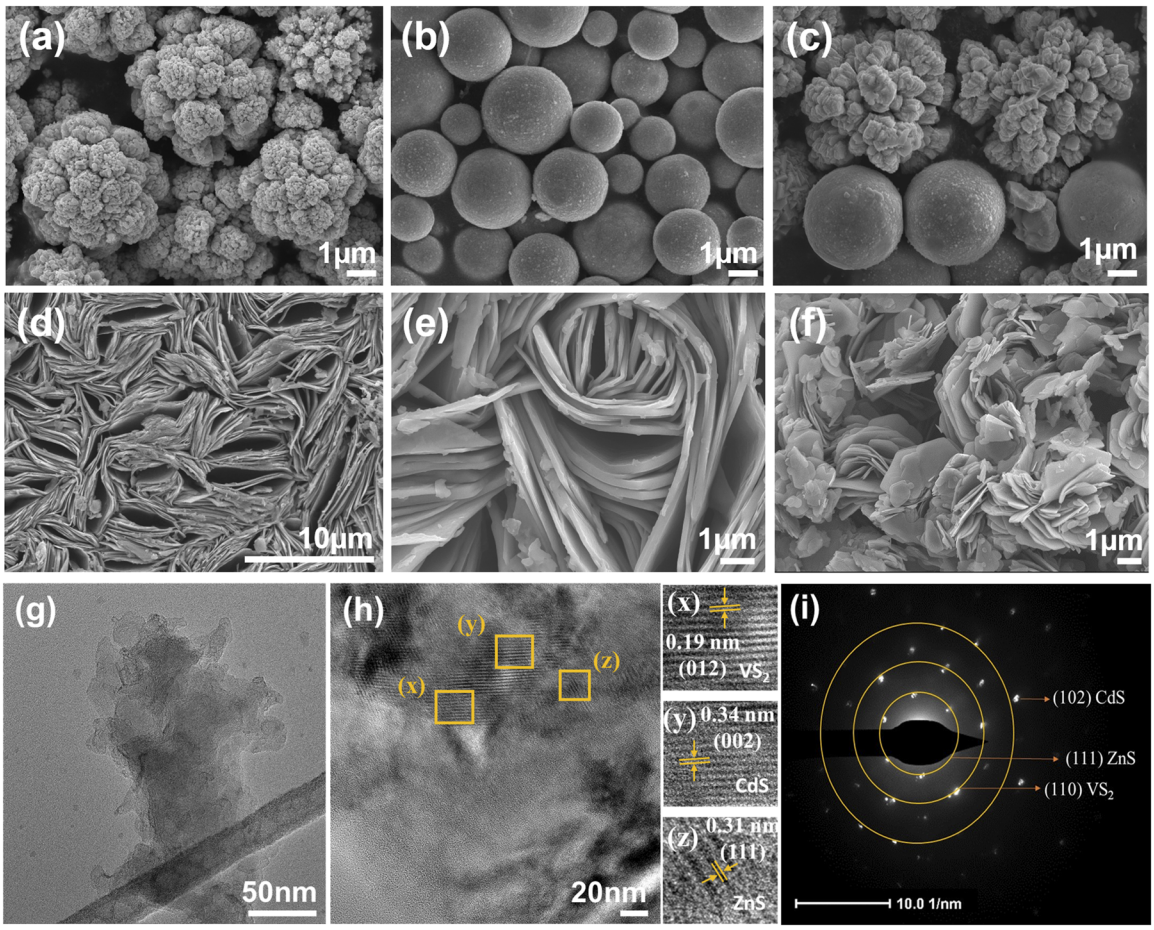

FIG. 4. FESEM images of (a) CdS, (b) ZnS, (c) ZnS/CdS, (d)–(e) VS_2, and (f) VS_2/ZnS/CdS. (g) TEM image of VS_2/ZnS/CdS, (h) HRTEM image of VS_2/ZnS/CdS, and (i) SAED pattern of VS_2/ZnS/CdS.

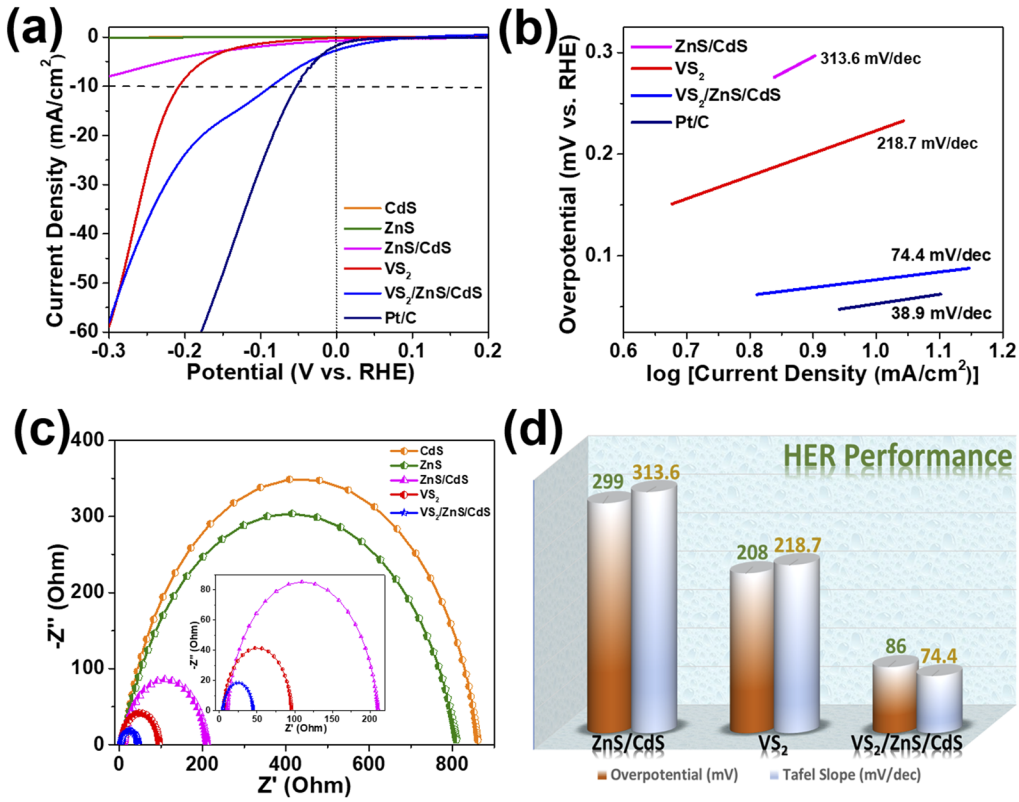

FIG. 5. Electrocatalytic HER performance of VS_2/ZnS/CdS: (a) LSV curves, (b) Tafel plots, (c) Nyquist plot, and (d) overall performance.

Pt/C catalyst. The commercial Pt/C shows the best catalytic activity for the HER with a small overpotential value (53 mV). In Fig. S4a, both pure ZnS and CdS present poor electrocatalytic performance, with large overpotential and low current densities. In contrast to pristine VS_2 (208 mV), the VS_2/ZnS/CdS hybrid exhibits a giant enhancement in HER activity, with an overpotential of ~86 mV at a generated catalytic current density of 10 mA/cm^2. The Tafel slope is a crucial intrinsic property of electrocatalysts and is directly related to the rate-limiting step of the HER. The electrocatalyst Pt/C, ZnS/CdS, VS_2, and VS_2/ZnS/CdS hybrid exhibit Tafel slope values of 38.9, 313.6, 218.7, and 74.4 mV/dec, respectively [Fig. 5(b)]. A lower Tafel slope of the VS_2/ZnS/CdS hybrid signifies the improved reaction kinetics for the HER. This is evident that the electrocatalytic ability was enhanced by the addition of the ZnS/CdS on VS_2, which facilitates H_2 desorption from its surface.

The equivalent electrical circuit used to model the HER process on the VS_2/ZnS/CdS hybrid GCE is shown in Fig. S4b and the experimental data are well fitted in Fig. 5(c). R_s represents the solution resistance of the system. The charge transfer resistance (R_{ct}) is related to the electrocatalysis kinetics and its lower value corresponds to a faster reaction rate. The arc of the EIS Nyquist plot specifies the charge transfer resistance, and a smaller arc radius indicates reduced charge transfer resistance. Furthermore, it reveals faster charge transportation from the electrode to the electrolyte. From the impedance result, it is clear that the R_{ct} of VS_2/ZnS/CdS hybrid is lower than that of VS_2 and other synthesized catalysts. Thus, it reveals that a decrease in the charge transfer resistance of the hybrid may due to the synergistic effect, which results in higher current density with an improved overpotential. The relative electrochemical active surface area (ECSA) of the catalysts is another key factor that affects the HER catalytic performance of electrocatalysts. Typically, C_{dl} is to be directly proportional to the catalytically active surface area of the electrode–electrolyte interface of electron transfer in the HER. The CV curves measured at various scan rates (Figs. S5a–S5c) and C_{dl} values have been calculated from the linear relationship of current density against the scan rate (Fig. S5d). The C_{dl} of the VS_2/ZnS/CdS hybrid is 12.7 mF/cm^2, which is five times larger than that of pristine VS_2 (2.3 mF/cm^2) and eight times larger than that of the ZnS/CdS structure (1.5 mF/cm^2). This indicates that the VS_2/ZnS/CdS hybrid possesses the larger catalytically relevant surface area.

Apart from the high HER activity, the stability of an HER catalyst is another practical parameter to consider when designing long-term operations. To evaluate the stability of the VS_2/ZnS/CdS hybrid structure in an acidic environment, we performed the current vs time measurements at constant overpotential for 8.33 h (Figs. S6a and S6b). After 8.33 h, the polarization curve maintains a similar shape to the initial one, with the same overpotential value. This suggests the high stability of the VS_2/ZnS/CdS hybrid structure electrode for long-term utilization. The FESEM

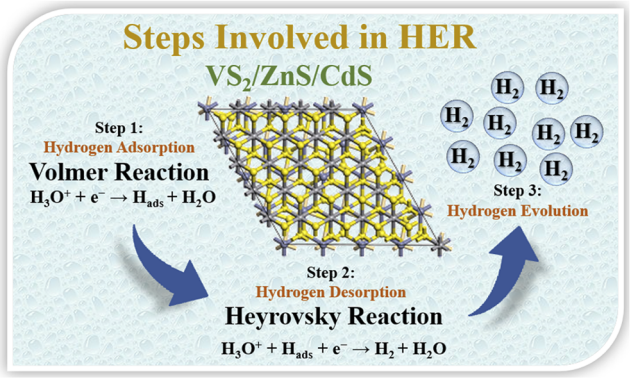

FIG. 6. Schematic illustration of the steps involved in HER performance of VS_2/ZnS/CdS.

images taken after the stability test are depicted in Figs. S7a and S7b, revealing that the catalyst still retains its fragmented sheet-like structure. Table S1 summarizes the electrochemical results of the VS_2/ZnS/CdS hybrid and the earlier reported V-based HER catalysts. One can see that the overpotential value for the VS_2/ZnS/CdS hybrid is lower than that for previously reported catalysts, and the Tafel value is also appreciable in comparison. This clearly explains the high performance of the VS_2/ZnS/CdS hybrid toward the electrocatalytic HER.

In acidic media, three key mechanisms have been suggested for the HER,[32]

(i) Volmer reaction ($H_3O^+ + e^- \rightarrow H_{ads} + H_2O$):

$$\mathbf{b} = \frac{2.3\mathbf{RT}}{\boldsymbol{\alpha}\mathbf{F}} \approx 120\ \text{mV/dec Tafel slope}, \tag{3}$$

where R is the ideal gas constant, T is the absolute temperature, $\alpha \approx 0.5$ is the symmetry coefficient, and F is the Faraday constant.

(ii) Heyrovsky reaction ($H_3O^+ + H_{ads} + e^- \rightarrow H_2 + H_2O$):

$$\mathbf{b} = \frac{2.3\mathbf{RT}}{(1+\boldsymbol{\alpha})\mathbf{F}} \approx 40\ \text{mV/dec Tafel slope}. \tag{4}$$

(iii) Tafel reaction ($2H_{ads} \rightarrow H_2$):

$$\mathbf{b} = \frac{2.3\mathbf{RT}}{2\mathbf{F}} \approx 30\ \text{mV/dec Tafel slope}. \tag{5}$$

As H_{ads} takes part in each electrochemical reaction step in the course of HER, it is important for judging the kinetics of HER. As compared to pristine VS_2, the decrease in the Tafel slope of the VS_2/ZnS/CdS hybrid indicates that there is a change in the rate-limiting reaction from the Volmer reaction to the partial Heyrovsky reaction. The Tafel slope (74.4 mV/dec) of the VS_2/ZnS/CdS hybrid suggests the Volmer–Heyrovsky mechanism as a major pathway for the HER.[32] The primary discharging step (Volmer reaction) for hydrogen adsorption is followed by the rate-determining electrochemical desorption of hydrogen gas (Heyrovsky reaction). The schematic illustration of the steps involved during the HER is portrayed in Fig. 6. The remarkable catalytic performance of the VS_2/ZnS/CdS hybrid structure for the HER is mainly attributed to the following: (i) the synergistic effects among VS_2, ZnS, and CdS; (ii) effectively increased exposed active sites for catalytic reactions than the bare structure; (iii) the excellent conductivity of VS_2 and ZnS/CdS accelerates electron and ion transport during the HER processes; and (iv) the strong interaction between VS_2, ZnS, and CdS.

To confirm the experimental findings on HER activity, we have calculated the free energy profile using DFT. Theoretically, Gibbs free energy is defined by the equation $\Delta G_H = \Delta E - T\Delta S + ZPE$, where ΔE denotes the change in total energy (calculated from DFT) and ΔS and ZPE represent a change in entropy and the zero-point energy difference between the adsorbed and the gas phase of hydrogen, respectively. However, the ΔS and ZPE of the adsorbed hydrogen are negligible to those of the gaseous phase at room temperature and ambient pressure. In our case, $T\Delta S - ZPE$ is about 0.27 eV. To define the free energy profile, an intermediate step of hydrogen adsorption (H^*) is important, while first (H^+) and final ($1/2H_2$) are expected to be in equilibrium.

As per experimental results, we have chosen the (1 0 1), (1 1 1), and (0 0 1) highest intensity XRD peak of CdS, ZnS, and VS_2 bulk structures. We have used the $5 \times 5 \times 1$, $4 \times 4 \times 1$ and $2 \times 4 \times 1$ supercell of VS_2 (0 0 1), ZnS (1 1 1), and CdS (1 0 1) planes. The lattice mismatch for the VS_2/ZnS heterostructure is 4.14% with respect to the

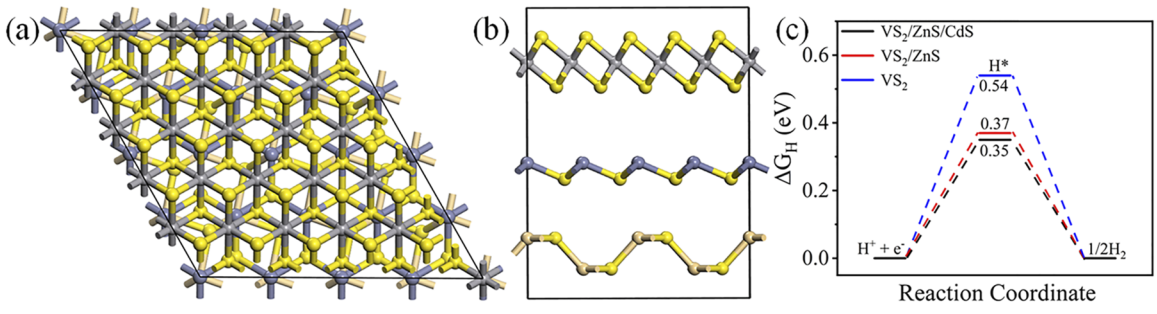

FIG. 7. (a) Top and (b) side view of VS_2/ZnS/CdS heterostructure and (c) the free energy diagram of HER the pristine and heterostructures.

VS_2 (0 0 1) plane. Next, we have used the same VS_2/ZnS heterostructure along with CdS (1 0 1) to mimic the VS_2/ZnS/CdS heterostructure. To understand the HER activity, we have studied three different structures named (i) VS_2, (ii) VS_2/ZnS, and (iii) VS_2/ZnS/CdS [Figs. 7(a) and 7(b)]. All the three structures have the first layer as VS_2, which has only sulfur as an active site. The free energy of hydrogen adsorbed ΔG_H for VS_2 is 0.54 eV, which well agrees with previous reports.[33] For the VS_2/ZnS heterostructure, ΔG_H is 0.37 eV. The effect of the CdS (1 0 1) layer is negligible because it is far from the VS_2 (0 0 1) layer that we have observed (ΔG_H: 0.35 eV) for the VS_2/ZnS/CdS heterostructure [Fig. 7(c)]. From the first-principles study, we found that VS_2/ZnS/CdS is more favorable in HER activity as compared to pristine VS_2.

IV. CONCLUSIONS

In summary, we report an efficient HER electrocatalyst, VS_2/ZnS/CdS hybrid structure, via a facile hydrothermal method. The VS_2/ZnS/CdS hybrid exhibits superior HER activity including high stability, low overpotential of 86 mV, and a smaller Tafel slope of 74.4 mV/dec under acidic conditions. The remarkable catalytic performance of the VS_2/ZnS/CdS hybrid is mainly attributed to the following: (i) the synergistic effect existing among VS_2, ZnS, and CdS; (ii) effectively increased active sites for catalytic reactions than a bare structure; (iii) excellent conductivity of VS_2 and ZnS/CdS, which accelerates electron/ion transport during the HER processes; and (iv) strong interaction between VS_2, ZnS, and CdS. Furthermore, DFT calculations theoretically confirm that the VS_2/ZnS/CdS hybrid structure favors HER because of its low hydrogen adsorption free energy (0.35 eV). Therefore, this work demonstrates that transition metal-based sulfides and their hybrids emerge as promising electrocatalysts for future high-performance energy conversion devices.

SUPPLEMENTARY MATERIAL

See the supplementary material for characterizations, CV and LSV curves, stability test, FESEM images, and a comparison table.

ACKNOWLEDGMENTS

The authors would like to acknowledge financial support from the SERB Early Career Research project (Grant No. ECR/2017/001850); Department of Science and Technology [Grant Nos. DST/NM/NT/2019/205(G) and DST/TDT/SHRI-34/2018]; Karnataka Science and Technology Promotion Society (Grant No. KSTePS/VGST-RGS-F/2018-19/GRD NO. 829/315); start-up grant, Jain University [Grant No. 11 (39)/17/013/2017SG]; Nanomission (Grant No. SR/NM/NS-20/2014) for the characterization facilities; and the Ministry of New and Renewable Energy, Government of India, under Grant No. 31/03/2014-15/PVSE-R&D for providing the computational facility. The authors also thank Mahendra Pawar, Sreeraj KA, and Rutuparna Samal for their help with sample characterization.

AUTHOR DECLARATIONS

Conflicts of Interest

The authors have no conflicts to disclose.

DATA AVAILABILITY

The data that support the findings of this study are available from the corresponding authors upon reasonable request.

REFERENCES

[1] B. You, M. T. Tang, C. Tsai, F. Abild-Pedersen, X. Zheng, and H. Li, "Enhancing electrocatalytic water splitting by strain engineering," Adv. Mater. **31**, 1807001 (2019).
[2] J. Hou, Y. Wu, B. Zhang, S. Cao, Z. Li, and L. Sun, "Rational design of nanoarray architectures for electrocatalytic water splitting," Adv. Funct. Mater. **29**, 1808367 (2019).
[3] L. Najafi, S. Bellani, R. Oropesa-Nuñez, B. Martín-García, M. Prato, V. Mazánek, D. Debellis, S. Lauciello, R. Brescia, Z. Sofer, and F. Bonaccorso, "Niobium disulphide (NbS_2)-based (heterogeneous) electrocatalysts for an efficient hydrogen evolution reaction," J. Mater. Chem. A **7**, 25593–25608 (2019).
[4] J. Wang, M. Yan, K. Zhao, X. Liao, P. Wang, X. Pan, W. Yang, and L. Mai, "Field effect enhanced hydrogen evolution reaction of MoS_2 nanosheets," Adv. Mater. **29**, 1604464 (2017).
[5] X. Han, X. Tong, X. Liu, A. Chen, X. Wen, N. Yang, and X.-Y. Guo, "Hydrogen evolution reaction on hybrid catalysts of vertical MoS_2 nanosheets and hydrogenated graphene," ACS Catal. **8**, 1828–1836 (2018).
[6] B. You and Y. Sun, "Innovative strategies for electrocatalytic water splitting," Acc. Chem. Res. **51**, 1571–1580 (2018).
[7] S. H. Yu, Z. Tang, Y. Shao, H. Dai, H. Y. Wang, J. Yan, H. Pan, and D. H. C. Chua, "*In situ* hybridizing MoS_2 microflowers on VS_2 microflakes in a one-pot CVD process for electrolytic hydrogen evolution reaction," ACS Appl. Energy Mater. **2**, 5799–5808 (2019).
[8] M. Chhowalla, H. S. Shin, G. Eda, L.-J. Li, K. P. Loh, and H. Zhang, "The chemistry of two-dimensional layered transition metal dichalcogenide nanosheets," Nat. Chem. **5**, 263–275 (2013).
[9] C. S. Rout, B.-H. Kim, X. Xu, J. Yang, H. Y. Jeong, D. Odkhuu, N. Park, J. Cho, and H. S. Shin, "Synthesis and characterization of patronite form of vanadium sulfide on graphitic layer," J. Am. Chem. Soc. **135**, 8720–8725 (2013).
[10] Q. Ji, C. Li, J. Wang, J. Niu, Y. Gong, Z. Zhang, Q. Fang, Y. Zhang, J. Shi, L. Liao, X. Wu, L. Gu, Z. Liu, and Y. Zhang, "Metallic vanadium disulfide nanosheets as a platform material for multifunctional electrode applications," Nano Lett. **17**, 4908–4916 (2017).
[11] P. He, M. Yan, G. Zhang, R. Sun, L. Chen, Q. An, and L. Mai, "Layered VS_2 nanosheet-based aqueous Zn ion battery cathode," Adv. Energy Mater. **7**, 1601920 (2017).
[12] S. Zhang, J. Wang, N. L. Torad, W. Xia, M. A. Aslam, Y. V. Kaneti, Z. Hou, Z. Ding, B. Da, A. Fatehmulla, A. M. Aldhafiri, W. A. Farooq, J. Tang, Y. Bando, and Y. Yamauchi, "Rational design of nanoporous MoS_2/VS_2 heteroarchitecture for ultrahigh performance ammonia sensors," Small **16**, 1901718 (2020).
[13] X. Zhong, J. Tang, J. Wang, M. Shao, J. Chai, S. Wang, M. Yang, Y. Yang, N. Wang, S. Wang, B. Xu, and H. Pan, "3D heterostructured pure and N-Doped Ni_3S_2/VS_2 nanosheets for high efficient overall water splitting," Electrochim. Acta **269**, 55–61 (2018).
[14] X. Wang, B. Shi, Y. Fang, F. Rong, F. Huang, R. Que, and M. Shao, "High capacitance and rate capability of a Ni_3S_2@CdS core–shell nanostructure supercapacitor," J. Mater. Chem. A **5**, 7165–7172 (2017).
[15] X. Hou, T. Peng, J. Cheng, Q. Yu, R. Luo, Y. Lu, X. Liu, J.-K. Kim, J. He, and Y. Luo, "Ultrathin ZnS nanosheet/carbon nanotube hybrid electrode for high-performance flexible all-solid-state supercapacitor," Nano Res. **10**, 2570–2583 (2017).
[16] A. D. Adhikari, R. Oraon, S. K. Tiwari, P. Saren, J. H. Lee, N. H. Kim, and G. C. Nayak, "CdS-$CoFe_2O_4$@reduced graphene oxide nanohybrid: An excellent electrode material for supercapacitor applications," Ind. Eng. Chem. Res. **57**, 1350–1360 (2018).
[17] R. Ramachandran, M. Saranya, P. Kollu, B. P. C. Raghupathy, S. K. Jeong, and A. N. Grace, "Solvothermal synthesis of Zinc sulfide decorated Graphene (ZnS/G) nanocomposites for novel Supercapacitor electrodes," Electrochim. Acta **178**, 647–657 (2015).

[18]W. Zhang, X. Chen, J. Zhang, C. Tuo, L. Ji, H. Li, X. Zhang, and F. Yang, "Exposure of active edge structure for electrochemical H_2 evolution from VS_2/MWCNTs hybrid catalysts," Int. J. Hydrogen Energy **43**, 22949–22954 (2018).
[19]K. Sekar, G. Raji, S. Chen, S. Liu, and R. Xing, "Ultrathin VS_2 nanosheets vertically aligned on $NiCo_2S_4$@C_3N_4 hybrid for asymmetric supercapacitor and alkaline hydrogen evolution reaction," Appl. Surf. Sci. **527**, 146856 (2020).
[20]X. Xiao, Y. Wang, X. Xu, T. Yang, and D. Zhang, "Preparation of the flower-like MoS_2/SnS_2 heterojunction as an efficient electrocatalyst for hydrogen evolution reaction," Mol. Catal. **487**, 110890 (2020).
[21]G. Kresse and J. Furthmüller, "Efficiency of ab-initio total energy calculations for metals and semiconductors using a plane-wave basis set," Comput. Mater. Sci. **6**, 15–50 (1996).
[22]J. P. Perdew, K. Burke, and M. Ernzerhof, "Generalized gradient approximation made simple," Phys. Rev. Lett. **78**, 1396 (1997).
[23]S. Grimme, "Semiempirical GGA-type density functional constructed with a long-range dispersion correction," J. Comput. Chem. **27**, 1787–1799 (2006).
[24]I. S. Amiinu, Z. Pu, X. Liu, K. A. Owusu, H. G. R. Monestel, F. O. Boakye, H. Zhang, and S. Mu, "Multifunctional Mo–N/C@MoS_2 electrocatalysts for HER, OER, ORR, and Zn–air batteries," Adv. Funct. Mater. **27**, 1702300 (2017).
[25]K. Hernandez Ruiz, J. Liu, R. Tu, M. Li, S. Zhang, J. R. Vargas Garcia, S. Mu, H. Li, T. Goto, and L. Zhang, "Effect of microstructure on HER catalytic properties of MoS_2 vertically standing nanosheets," J. Alloys Compd. **747**, 100–108 (2018).
[26]K. Karthick, T. K. Bijoy, A. Sivakumaran, A. B. Mansoor Basha, P. Murugan, and S. Kundu, "Enhancing hydrogen evolution reaction activities of 2H-phase VS_2 layers with palladium nanoparticles," Inorg. Chem. **59**, 10197–10207 (2020).
[27]X. Li, M. Li, J. Yang, X. Li, T. Hu, J. Wang, Y. Sui, X. Wu, and L. Kong, "Synergistic effect of efficient adsorption g-C_3N_4/ZnO composite for photocatalytic property," J. Phys. Chem. Solids **75**, 441–446 (2014).
[28]A. Goktas and İ. H. Mutlu, "Structural, optical, and magnetic properties of solution-processed co-doped ZnS thin films," J. Electron. Mater. **45**, 5709–5720 (2016).
[29]P. P. Bag, X.-S. Wang, P. Sahoo, J. Xiong, and R. Cao, "Efficient photocatalytic hydrogen evolution under visible light by ternary composite CdS@NU-1000/RGO," Catal. Sci. Technol. **7**, 5113–5119 (2017).
[30]S. Velanganni, S. Pravinraj, P. Immanuel, and R. Thiruneelakandan, "Nanostructure CdS/ZnO heterojunction configuration for photocatalytic degradation of Methylene blue," Physica B **534**, 56–62 (2018).
[31]D. Gao, Q. Xue, X. Mao, W. Wang, Q. Xu, and D. Xue, "Ferromagnetism in ultrathin VS_2 nanosheets," J. Mater. Chem. C **1**, 5909–5916 (2013).
[32]Y. Li, H. Wang, L. Xie, Y. Liang, G. Hong, and H. Dai, "MoS_2 nanoparticles grown on graphene: An advanced catalyst for the hydrogen evolution reaction," J. Am. Chem. Soc. **133**, 7296–7299 (2011).
[33]S. Yang, J. Kim, Y. J. Tak, A. Soon, and H. Lee, "Single-atom catalyst of platinum supported on titanium nitride for selective electrochemical reactions," Angew. Chem., Int. Ed. **55**, 2058–2062 (2016).